Abstract for the 30th International Workshop on Water Waves and Floating Bodies, Bristol (UK), 12 – 15 April, 2015

On the modeling of nonlinear wave-wave and wave-body interactions in a realistic sea state

Wei Bai*, Xingya Feng, Xianglong Chen and Kok Keng Ang
Department of Civil and Environmental Engineering, National University of Singapore, Singapore
E-mail: w.bai@nus.edu.sg

Highlights:

- A time-domain nonlinear potential model is developed to solve wave-body interactions in a realistic sea state.
- Nonlinearity is demonstrated through simulating focused waves and wave diffraction by side-by-side barges subject to an irregular wave field.

1. Introduction

This abstract aims to present a nonlinear potential flow model which generates a realistic sea state and solves wave-body interaction problems. The fully nonlinear potential flow theory (FNPF) remains one of the advanced and efficient methods to model water waves and wave-body interactions. Recently, various numerical models have been developed in order to implement FNPF efficiently. Engsig-Karup *et al.* [1] presented a higher-order finite difference (FD) model, *OceanWave3D*, which was proved very accurate in simulating wave-wave and wave-body interactions by comparisons against experiments. Guerber *et al.* [2] presented a two-dimensional model with a freely or forced moving submerged horizontal cylinder and solved the boundary value problem by a higher-order boundary element method (HOBEM), which was simulated to represent the wave energy converters (WECs). Targeted at improving the computational efficiency, Shao and Faltinsen [3] developed a new 3D FNPF model based on harmonic polynomial cells. The computational domain is discretized by harmonic polynomials such that velocity potential at each field point is interpolated by a set of harmonic polynomials. However, these models focus much on modelling regular wave fields. Ducrozet *et al.* [4] presented a modified higher-order spectral (HOS) nonlinear potential model with a controlled wave maker. The key point in the modified model is wave generation by an additional potential which satisfies the no-flux condition on wave maker and nonlinear free surface conditions. Validation cases of 2D irregular waves and 3D focused waves illustrate high accuracy with comparisons against experimental data.

In this abstract, we present a 3D FNPF model based on HOBEM and focus on modelling irregular wave fields and wave-body interactions in a realistic sea state. One of our concerns is the associated nonlinearity which is yet much discussed in the previous work.

We first simulate a 2D focused wave in a rectangular numerical wave tank (NWT). Of interest is the presence of higher frequency components induced by nonlinear wave-wave interactions, which however cannot be identified in linear models. To improve computational efficiency, we modified the rectangular NWT into a circular tank. In the modified tank, no wave maker is modelled; instead, we impose an irregular wave field as an incoming wave. Only the scattered wave field needs to be solved. To demonstrate its capacity, we simulate a case of two side-by-side barges in a realistic sea state and comparisons with model tests are presented. The nonlinearity in the wave response is investigated.

2. Numerical model

2.1 Rectangular NWT

Following the basic assumptions of FNPF theory, i.e. fluid is incompressible, inviscid and flow irrotational, the velocity potential $\phi(x,y,z,t)$ satisfies the Laplace equation in the domain,

$$\nabla^2\phi = 0\,. \tag{1}$$

On the free water surface S_F, the kinematic and dynamic boundary conditions in the Lagrangian description are

$$\frac{\mathrm{D}\mathbf{X}}{\mathrm{D}t} = \nabla\phi\,, \tag{2}$$

$$\frac{\mathrm{D}\phi}{\mathrm{D}t} = -gz + \frac{1}{2}\nabla\phi\cdot\nabla\phi\,, \tag{3}$$

where D/Dt is the material derivative, $\mathbf{X}$ denotes the position of water particles on the free water surface. On solid walls, non-flux condition is satisfied.

A wave maker is located at one end of the rectangular tank, and a numerical beach is placed at the other end to avoid reflection from the end wall. In order to generate any desired irregular wave field, we need to specify the movement of wave maker (piston type). Given any targeted wave spectrum $S(\omega)$ (discretized into N harmonics), the displacement of wave maker is specified as

$$x_{WM}(t) = \sum_{n=1}^{N} \sqrt{2S_{WM}(\omega_n)\Delta\omega} \cos(k_n x_p - \omega_n t + p_n)\,, \quad (4)$$

$$S_{WM}(\omega_n) = e_0 S(\omega_n)\,, \quad (5)$$

$$e_0 = \frac{4\sinh^2(k_n h)}{2k_n h + \sinh(2k_n h)}\,, \quad (6)$$

where e_0 is a transfer function; ω_n is the wave frequency, k_n the wave number, and p_n the phase offset of the nth component. In addition, h is the water depth and $\Delta\omega$ is the frequency interval. x_p is a reference position, and in the case of focused waves it is the focal point. More details on the irregular wave generation can be found in Frigaard *et al.* [5].

2.2 Circular tank model

While modelling wave-body interaction problems using the above rectangular NWT, the side wall effect becomes significant, unless in a very wide tank which requires huge computational effort. In order to eliminate tank wall effects and improve computational efficiency, we develop a nonlinear decomposition model which solves wave-body interactions in a circular tank. In the decomposition model, the incident wave field is specified explicitly while only the scattered wave is solved instead of computing the original total wave.

The total velocity potential $\phi(x,y,z,t)$ can be separated into an incident wave part and a scattered part, i.e. $\phi = \phi_I + \phi_S$. The free surface is updated from the contributions of incident and scattered velocities. The incident flow potential and velocities are evaluated explicitly in the fluid domain. By substituting the separation of potential and elevation into Eqns. (1), (2) and (3), the decomposition leads to the following boundary value problem (BVP) for the scattered component:

$$\nabla^2 \phi_S = 0\,, \quad (7)$$

with boundary conditions on free surface:

$$\frac{\mathrm{D}\mathbf{X}_S}{\mathrm{D}t} = \nabla\phi - \nabla\phi_I \text{ , on } S_F \quad (8)$$

$$\frac{\mathrm{D}\phi_S}{\mathrm{D}t} = -gz_S + \frac{1}{2}\nabla\phi\cdot\nabla\phi - \frac{1}{2}\nabla\phi_I\cdot\nabla\phi_I \text{ , on } S_F \quad (9)$$

and on body surfaces:

$$\frac{\partial\phi_S}{\partial n} = -\frac{\partial\phi_I}{\partial n} \text{ , on } S_B \quad (10)$$

where the subscripts '*I*' and '*S*' denote the components of incident and scattered waves respectively.

The generation of a realistic sea state is similar to that in the rectangular wave tank, except that there is no wave maker in this circular tank. Once the energy spectrum is chosen, the free surface elevation and the velocity potential can be calculated as a sum of N (N should be large enough to reproduce the desired spectrum) harmonics,

$$z_I(x,t) = \sum_{n=1}^{N} A_n \cos(k_n x - \omega_n t + p_n), \quad A_n = \sqrt{2S(\omega_n)\Delta\omega}, \quad (11)$$

$$\phi_I(x,z,t) = \sum_{n=1}^{N} A_n \frac{\omega_n}{k_n} \frac{\cosh k_n(z+h)}{\sinh k_n h} \sin(k_n x - \omega_n t + p_n)\,, \quad (12)$$

where A_n is the amplitude of the nth wave component. The phase is a random function following the standard uniform distribution, ranging from 0 to 2π. No transfer function is required due to the nature that no wave maker is used in this model.

A higher-order boundary element method (HOBEM) is employed to simulate the wave-body interactions in the time domain. Time integration is performed via the 4th order Runge-Kutta scheme, and free surface conditions are updated based on a Mixed Eulerian -Lagrangian scheme.

3. 2D Focused waves

We employ the rectangular NWT presented in Section 2.1 to simulate 2D focused waves. In our higher-order boundary element simulations, the focused waves (Case D55) are performed in a water depth of 0.7 m, of which the nonlinearity has been validated through comparison with the experimental results in Baldock *et al.* [6]. The wave conditions are designed according to the configuration of Case D (with the input amplitude of 55mm) in Baldock *et al.* [6]. The wave group is comprised of 29 individual wave components and they are subject to a spectrum within a wave period range (0.8 - 1.2s).

The time history of the simulated wave elevation at focal point is compared with the experimental data as shown in Fig. 1 and the linear prediction is also included. A good agreement is achieved between the present numerical result and the experimental data, while the linear prediction is different from them. It is observed that the discrepancy is especially remarkable at the focused crest. This may be due to the contribution of nonlinear interaction between different wave components during the wave propagation. Fig. 2 shows the normalized power spectra derived from the data of the three time histories shown in Fig. 1. The normalized power spectrum of the present numerical result (black solid line) is very close to that of the experimental result (black dot line), though both of them significantly diverge from the spectrum derived from the linear prediction (gray dash line). There is a minor energy leakage towards the lower harmonics, while a large amount of energy is transferred to the higher harmonics. The significant redistribution of the wave energy is clearly identified and again confirms that the energy transferred into higher harmonics mainly results in the crest discrepancy shown in Fig. 1. This may suggest that

the nonlinear wave-wave interaction, which is one of the essential features in the realistic irregular wave field, is also incorporated in the present numerical wave model.

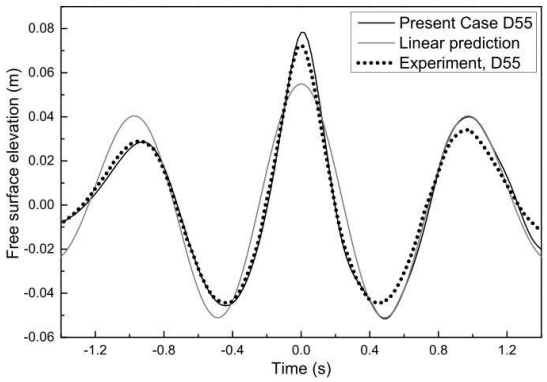

Fig. 1. Comparisons of the time history of wave elevation at the focal point

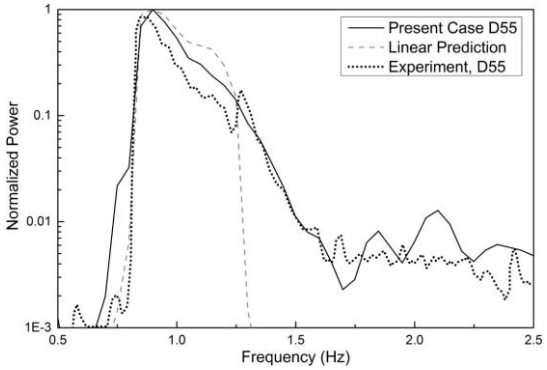

Fig. 2. Normalized power spectra derived from the time histories

4. Twin-barge in irregular waves

The circular tank model presented in Section 2.2 is employed to simulate wave-body interaction problems. The problem of gap resonance has attracted much attention recently due to unrealistic predictions of wave response from linear models. We consider a case of two side-by-side rectangular barges, which has been investigated in Molin *et al*. [7]. The configuration of the side-by-side barges at model scale is as follows: barge length is 2.47 m, width 0.6 m, draft 0.18 m and gap width 0.12 m. The water depth is set as 3 m (the same as in the tests), and the tank radius for the present simulations is either 5 m or four times the incident wave length, whichever is larger. The incident wave heading considered here is 90 degrees, i.e. beam sea. In the experiments in Molin *et al*. [7], the barges are fixed and subject to an irregular sea state with the Pierson-Moskowitz spectrum of a significant wave height H_s = 0.02 m and a peak period T_p = 1 s. In our simulations, we utilize the same PM spectrum, and consider only the beam sea situations. The frequency range is truncated to 3~20 rad/s which covers more than 95% of the energy. The number of wave components is N = 480 which is large enough for the accurate reproduction of the targeted spectrum. With a small time step in the long time simulations, no numerical instability was encountered despite of inclusion of some short-period wave components. A typical time history of output surface elevation in the gap at midship is plotted in Fig. 3, which is normalized by the significant wave amplitude A_s (defined as half the significant wave height here).

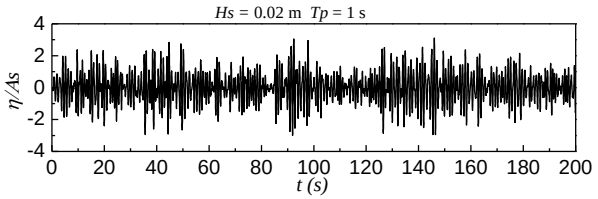

Fig. 3. Time history of elevation in the gap at midship with side-by-side barges in beam sea subject to a PM spectrum

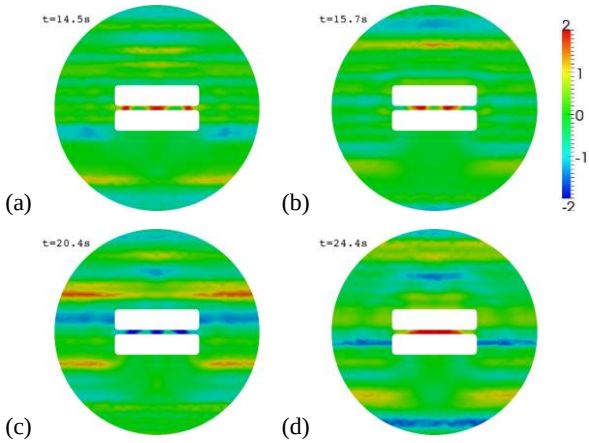

Fig. 4. Contours of free surface elevations near the barges subject to irregular waves at different time instants: (a) t =14.5 s; (b) t = 15.7 s; (c) t = 20.4 s and (d) t = 24.4 s

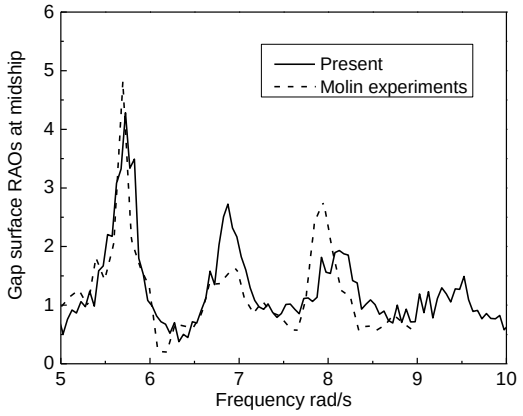

Fig. 5. Free surface RAOs in the gap at midship with barges in beam sea subjected to PM spectrum of H_s = 0.02 m and T_p = 1 s

An overview of the free surface elevations near the barges at some time instants is shown in Fig. 4. Although the surface elevations along the wave propagating direction (unidirectional incident wave) are

mostly random, some peak regions can be clearly recognized within the gap at certain time instants, which indicates the possible trapping or resonant phenomenon. For instance, at t = 14.5 s in Fig. 4(a) we can observe three peak regions distributed along the narrow gap; and at t = 24.4 s the whole surface in the gap tends to be high except at the two openings. This figure implies that in random wave simulations wave in the gap may experience all the possible resonant modes at different time instants in one run if the numerical model is fine enough and the simulation runs for an enough long time.

A close investigation ought to be done by spectral analysis, in order to make a direct comparison against the experimental results in Molin *et al.* [7]. To obtain response RAOs, cross spectral analysis is utilized in processing the recorded time histories of the present simulations. However, with a single set of record of signals, the generated energy spectrum tends to be raw with large errors. To achieve a convergent results from the statistical point of view, we repeat the run for ten times and each run contains 200 s simulating time, with considering the computing resources. The resulting RAOs are predicted by averaging the results in these ten runs. One must bear in mind that in this process information within the small frequency interval of 1/200 Hz might be missing according to the current adopted simulating time and sampling rate.

Fig. 5 shows the response RAOs of the surface elevation in the gap at midship with side-by-side barges in beam sea. It can be seen that our results demonstrate a similar character to that of the experiments, where several peaks are formed at certain frequencies. These peaks are corresponding to the associated wave resonances in the gap. The resonant frequencies are well captured at these peaks in Fig. 5, and the overall agreement of RAO values with the experiments is favorable except at the second and third peaks. Our simulation generates a higher value at the second peak, but a lower one at the third peak than the experiments. It is noticed that the present frequency range near resonances tend to be broader at higher modes, and the peak values are reduced at higher modes compared to that at lower ones, which seem reasonable. A fourth peak is also formed near the frequency 9.5 rad/s, however this mode is even broader and the peak value is much lower compared to the first mode. The simulation in irregular waves, as in the experiments, can successfully capture the possible resonant modes, the accuracy, anyhow, is limited by the fact that the responses are extracted from time recordings at corresponding positions through spectral analysis. This is sensitive in regard to obtaining precise RAOs with a small frequency interval (this is similar to that in the experiments, as commented by Molin *et al.* [7]).

As far as the nonlinearity concerns, we impose an irregular sea state of low significant wave height Hs = 0.002 m as the incident wave. We repeat the case with the same parameters including the random phases of every wave components in the incident wave, except for the significant wave height. A comparison of wave elevation in the gap at midship is presented in Fig. 6 for these two spectra. Both elevations are normalized by significant wave amplitude A_S. The difference between the elevations can be explained by the nonlinearities in the decomposition model, although the incident wave fields are represented by linear wave combinations. This suggests that the present decomposition model is able to capture nonlinear effects despite of adopting a simple irregular wave model as the incident wave.

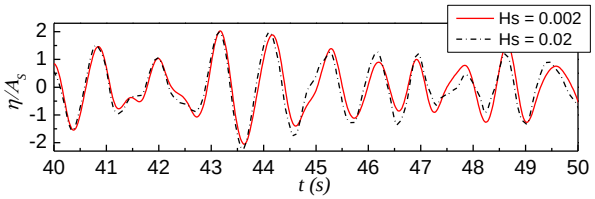

Fig.6. Comparison of wave elevation in the gap at midship for spectra of different significant wave heights

5. Conclusions

We demonstrate the accuracy of a nonlinear potential flow model by simulating focused waves. The nonlinearity in wave-wave interactions explains the discrepancy between linear prediction and experiments. Capability of a nonlinear decomposition model is illustrated by modelling the case of side-by-side barges subject to a realistic sea state. Nonlinearity associated with wave-body interactions is also identifies.

References

[1] Engsig-Karup, A.P. Bingham, H.B., Lindberg. O. 2009. An efficient flexible-order model for 3D nonlinear water waves. *Journal of Computational Physics*, Vol. 228, pp. 2100-2118.

[2] Guerber, E., Benoit, M., Grilli, S.T., Buvat, C. 2012. A fully nonlinear implicit model for wave interactions with submerged structures in forced or free motion. *Engineering Analysis with Boundary Elements*, Vol. 36, pp. 1151-1163.

[3] Shao, Y.L., Faltinsen, O.M. 2014. A harmonic polynomial cell (HPC) method for 3D Laplace equation with application in marine hydrodynamics. *Journal of Computational Physics*, Vol. 274, pp. 312-332.

[4] Ducrozet, G., Bonnefoy, F., Le Touze, D., Ferrant, P. 2012. A modified high-order spectral method for wavemaker modeling in a numerical wave tank. *European Journal of Mechanics B-Fluids*, Vol. 34, pp. 19-34.

[5] Frigaard, P., Hgedal, M., Christensen, M. 1993. Wave generation theory. Hydraulic & Coastal Engineering Laboratory, Department of Civil Engineering, Aalborg University, Aalborg, Denmark.

[6] Baldock, T.E., Swan, C., Taylor, P.H. 1996. A laboratory study of nonlinear surface waves on water. *Philos Trans R Soc Lond Ser A*, Vol. 354, pp. 649–76.

[7] Molin, B., Remy F., Camhi, A., Ledoux, A. 2009, Experimental and Numerical Study of the Gap Resonances in-between Two Rectangular Barges, *Proc. of 13th Cong. of International Maritime Association of Mediterranean IMAM*, (Istanbul).